Acoustic and Biomedical Engineering

Construction of Equivalent Models of Continuous and Discrete-Continuous Systems

S. Kasprzyk and R. Marczuk

AGH University of Science and Technology, Faculty of Mechanical Engineering and Robotics

Department of Mechanics and Vibroacoustics, al. A. Mickiewicza 30, 30-059 Krakow, Poland

New models have been constructed for three physical systems. These models are characterized by a uniform and transparent mathematical description. The mathematical description belongs to the class of generalized functions, which means that all equations as well as their solutions are understood in the sense of weak topology. The elements of the set of generalized functions need not be differentiable (in the classical sense) at each point domain of the function. Analyzing of actual systems in the class of generalized functions does not require a division into subsystems, which simplifies significantly execution of all mathematical operations. As compared with the classical methods, those presented in the study allow for a much faster achievement of the goal.

PACS: 46.70.De, 46.40.−f

1. Introduction

Examination of physical systems mostly consists in construction of a model that can be mathematically described in a relatively simple way. The choice of such a model need not be unique, although each of them allows for the achievement of the defined goal. The paper presents construction of mathematical models of actual continuous and discrete-continuous systems whose mathematical description belongs to the class of generalized functions [1–4]. Model A and model B are treated as equivalent if they realize the same goal. The considerations regard boundary value and initial-boundary value problems. Three physical systems of changeable structure were presented, for which equivalent mathematical models were constructed:

1.1. The first system: Euler's beam with step changes of stiffness

Stiffness of systems is constant at intervals; moreover, for the interval $\langle 0, a) \cup (b, l\rangle$ it has a finite value and in the interval $\langle a, b\rangle$ the value is much higher than in the remaining intervals.

Model one. Classical model, based on the classical mathematical analysis was constructed by dividing a beam into three subsystems, that is $\langle 0, a)$, $\langle a, b\rangle$ and $(b, l\rangle$. Each of the subsystems is analyzed separately in the aspect of the determined goal, and concatenation of the solutions is executed subsequently.

Model two. This model was constructed by substituting the interval $\langle a, b\rangle$ with a one-point interval $\{a\}$ and adding an appropriate force $\boldsymbol{Q}$ acting at the point a, and an appropriate couple of forces with the moment $\boldsymbol{M}$. The force $\boldsymbol{Q}$ and the couple of forces $\boldsymbol{M}$ are selected in such a way that the reactions of the beam supports are not changed.

Model three. The construction of this model consists in applying of a beam with constant stiffness in its full length l, while the interval $\langle a, b\rangle$ is additionally loaded with an appropriate infinite sequence of force couples that do not change the reaction of the beam supports.

1.2. The second system: a typical discrete-continuous system

This system consists of Euler's beam (a continuous system) with the following parameters: density ρ, cross-section area F, bending stiffness EJ, internal dumping coefficient α, length l, and of a discrete system with one degree of freedom with the discrete parameters: mass m, stiffness k, damping coefficient h, moving on the straight line perpendicular to the beam axis (see Fig. 1).

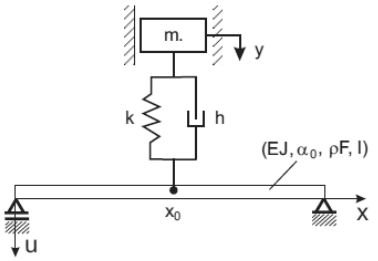

Fig. 1. A model of a typical discrete-continuous system.

The discrete system is connected to the beam (the continuous system) with linear elastic-dissipative constraints at the point x_0. Mathematical description leads to a system of differential equations with distributive coefficients, therefore such systems can be analyzed in the class of generalized functions. An analysis of linear continuous-discrete systems is performed conveniently and easily with the use of the Fourier method. This method leads to separation of variables for a certain relation between the parameters E, α, k and h. If the parameters of the system do not satisfy this relation, the analysis of vibrations can be conducted in two ways.

Model one. In this model we execute a division of the discrete-continuous system into three subsystems:

1. a continous system $\langle 0, x_0 - \epsilon)$; $0 < \epsilon < \epsilon_0$
2. a discrete system with two degrees of freedom, with parameters: m, k, h, $\rho F \cdot 2\epsilon$;
3. a continous system $(x_0 + \epsilon, l\rangle$, $0 < \epsilon < \epsilon_0$.

The analysis of vibration in these subsystems is performed in a standard way [5], with additional geometrical conditions. Subsequently, the results are "combined" at the points $x_0 - \epsilon$ and $x_0 + \epsilon$.

Model two. The model does not require a physical division into subsystems. Thanks to a certain modification of the method of separation of variables the solution is acquired in the class of generalized functions [6].

1.3. The third system: Euler's beam with a crack

Another physical system that is taken into consideration is Euler's beam with the parameters ρF. EJ, α, l with the typical boundary conditions and a crack perpendicular to the beam axis at the point x_0. The problem considered is the influence of the crack depth caused on the transverse vibrations of the system [7, 8]

Model one. The model known from literature, in which the undamaged part of the cross-section at the crack is replaced with an appropriate spring [7]. For this model the first frequency of vibrations is determined depending on the depth of the crack. It turns out that the first frequency of the beam's own vibrations is a decreasing function of the depth of the crack.

Model two. This model is constructed on the base of an algebraic equation whose roots are eigenvalues. It should be mentioned that it is a more general form of the equation of transverse vibrations of Euler's beam than those found in literature [6]:

$$\frac{\partial^3}{\partial x^3}\left[EJ(x)\left(\frac{\partial u}{\partial x} + \frac{\alpha}{E}\frac{\partial^2 u}{\partial x \partial t}\right) + \rho F(x)\right]\frac{\partial^2 u}{\partial t^2} = q(x,t). \tag{1}$$

The equation is derived on the basis of an analysis of the natural vibrations of the beam with the step change of stiffness in the area of the point x_0. The decrease of stiffness is modeled by

$$[H(x_0 - \epsilon) - H(x_0 + \epsilon)]EJ\gamma_1, \tag{2}$$

where $H(a)$ is a Heaviside step function with step at point a, $-1 < \gamma_1 \leq 0$. The loss of cross-section area is modeled by

$$[H(x_0 - \epsilon) - H(x_0 + \epsilon)]\rho F\gamma_2, \tag{3}$$

where $-1 < \gamma_2 \leq 0$.

Model three. It consists in an analysis of natural vibrations of a certain discrete-continuous system (with Euler's beam as the continuous system). In this case an increase of stresses takes place in the area of the point x_0. This local increase of stresses is caused by application of two pairs of forces (of equal values) at the points: $x_0 - \epsilon$, $x_0 + \epsilon$, where $0 < \epsilon$, ϵ — thickness of the crack.

2. Diagrams of the systems and their mathematical descriptions

2.1. Euler's beam with a step change of stiffness

This system has been presented in Fig. 2. We assume that in the intervals $\langle 0, a)$ and $(b, l\rangle$ stiffness equals $\beta > 0$, while in the interval $\langle a, b\rangle$ the beam is a rigid body, that is, its stiffness is infinite.

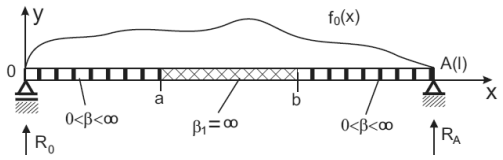

Fig. 2. Euler's beam with a step change of stiffness.

f_0 is distribution of external force in the plane xy — acting on the beam The equation of bending line of the beam presented in Fig. 2 can be obtained in three ways:

1. based on the classical mathematical analysis without using the distribution (4) (*model one*, not described here);
2. with the use of the distribution (4) and the division into three subsystems corresponding with the intervals: $\langle 0, a)$, $\langle a, b\rangle$ and $(b, l\rangle$;
3. substitution of the interval $\langle a, b\rangle$ with one-point interval: $\langle 0, a) \cup \{a\} \cup (b - a, l - (b - a))\rangle$. The model of a beam corresponding with (3.) is presented in Fig. 3.

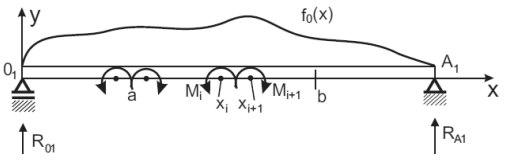

Fig. 3. Model 2 of Eluer's beam with step change of stiffness.

2.1.1. Model Two

Distribution of external force and support reactions (4):

$$\Psi_0(x) = R_0\delta_0(0) + f_0(x) + R_A\delta_l(l). \tag{4}$$

It is easy to check that [6]:

$$\int_{-\infty}^{x} \Psi_{i-1}(u)\,\mathrm{d}u = \Psi_i(x), \quad i = 1, 2, 3, 4, \tag{5}$$

static equation of equilibrium

$$\Psi_1(l) = 0, \quad \Psi_2(l) = 0. \tag{6}$$

From Eq. (6) it follows that:

$$R_0 = \frac{1}{l}f_2(l), \tag{7}$$

$$R_A = \frac{1}{l}f_2(l) - f_1. \tag{8}$$

The distribution of forces for the model represented in Fig. 3 [6] in the form (9):

$$\tilde{\Psi}_0(x) = R_0\delta_0 + f_0(x)\big[H_0 - H_a^-\big] + Q\delta_a + M0\delta_a' + \frac{b-a}{l} f_2(l)\delta_c' + f_0(x+(b-a))H_a^+ + R_A\delta(l), \quad 0 \le c \le l_1 \tag{9}$$

causes that

$$\boldsymbol{R}_0 = \boldsymbol{R}_\mathbf{0}', \quad \boldsymbol{R}_A = \boldsymbol{R}_A'. \tag{10}$$

The distribution (9) ensures continuity of the bending line of the beam shown in Fig. 3, while the distribution in the form (11):

$$\Phi_0(x) = \tilde{\Psi}_0(x) + K\delta_a''. \tag{11}$$

where K is a certain constant, causes discontinuity of the bending line of the beam from Fig. 3.

Let us determine the equation of the bending line of the axis of the beam shown in Fig. 3 with the distribution of forces (11). Then let us shift the diagram of the bending line of the beam corresponding with $(b, l\rangle$ to the right by the segment $b-a$. Later we should connect the right hand end of the diagram corresponding with $\langle 0, a)$ with the left hand end of the diagram corresponding with $(b, l\rangle$ with the help of a straight line segment. In this way we obtain the diagram of the bending line of the axis of the beam from Fig. 3. Let us determine

$$F(d)H_a^- := F(a^-)H_a, \quad F(d)H_a^+ := F(a^+)H_a, \quad d \le a, \tag{12}$$

where H_a^-, F_a^- mark the left-hand limits in a; H_a^+, F_a^+ — the right hand limits in a.

Differential equations of particular segments of the beam (2):

$$\begin{cases} \beta y_1''(x) = \tilde{\Psi}_2(x), & 0 \le x < a, \\ \beta y_2'' \equiv 0, & a \le x \le b, \\ \beta y_3''(x) = \tilde{\Psi}_2(x), & b < x \le l, \end{cases} \tag{13}$$

or after double integration

$$y(x) = \tag{14}$$

$$\begin{cases} \beta y_1(x) = -\frac{1}{l} f_2(l)\frac{(x-0)^3}{6} H_0 + f_4(x) + C_1 x + C_2, \\ \qquad 0 \le x < a, \\ \beta y_2(x) = D_1 x + D_2, \\ \qquad a \le x \le b, \\ \beta y_3(x) = -\frac{1}{l} f_2(l)\frac{(x-0)^3}{6} H_0 + f_4(x) + C_3 x + C_4, \\ \qquad b < x \le l. \end{cases}$$

Boundary value and geometric boundary conditions:

$$y(0) = y_1(0) = 0, \quad y(l) = y_3(l) = 0, \quad y_1'(a^-) = D_1, \quad y_3'(b^+) = D_1, \quad y_1(a^-) = D_1 a, \quad D_1 a = y_3(b^+); \quad C_2 = 0, \quad C_1 = C_3. \tag{15}$$

We shall derive the remaining constants from the equations

$$C_4 + K = (b-a)D_1,$$

$$D_1 a + D_2 - C_1 a = -\frac{1}{l} f_2(l)\frac{a^3}{6};$$

$$C_1 - D_1 = +\frac{1}{l} f_2(l)\frac{a^2}{2} - f_3(a^-),$$

$$C_1 l + C_4 K = f_2(l)\frac{l^2}{6} + f_4(l) \tag{16}$$

obtained from the model in Fig. 3 with the use of the distribution (11).

2.1.2. Model Three

For Euler's beam with the step change of stiffness (2) without a division into subsystems, the bending line of the axis of the beam will be determined. We will substitute the beam from the model shown in Fig. 2 with a uniform beam, and in the interval $\langle a, b\rangle$ we apply an appropriate sequence of force couples, which is shown in Fig. 4.

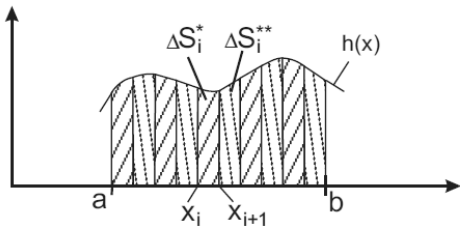

Fig. 4. Model 3 of Euler's beam with step change of stiffness.

The distribution of active forces (17) and reactions of the supports for Fig. 3:

$$\tilde{\Psi}_0(x) = R_0\delta_0 + f_0(x) + R_A\delta_A. \tag{17}$$

Models shown in Fig. 2 and Fig. 3 are equivalent for $a = x_1$, $b = x_n$.

The sequence of force couples $\{(\bar{M}_k, \bar{M}_{k+1})\}$, $k = 1, 2, \ldots n$ in the model in Fig. 4:

$$\beta = EJ, \quad \bar{R}_0 = \bar{R}_{01}, \quad \bar{R}_A = \bar{R}_{\mathrm{A1}}$$

must satisfy the condition (18):

$$\boldsymbol{M}_k + \boldsymbol{M}_{k+1} = \mathbf{0}, \quad \boldsymbol{M}_k = [0, 0, M_k];$$

$$\lim_{n\to\infty} \sum_{i=1}^{n} \big(M_{2i-1}\delta_{2i-1}' + M_{2i}\delta_{2i}'\big). \tag{18}$$

The distribution of external forces and support reactions for the model in Fig. 4 has the form (19):

$$\varphi_0 = R_0\delta_0 + f_0(x) + R_A\delta_A + \lim_{n\to\infty} \sum_{i=1}^{n} \big(M_{2i-1}\delta_{2i-1}' + M_{2i}\delta_{2i}\big), \tag{19}$$

where $M_{2i-1} = -a_{2i-1}$, $\lim_{n\to\infty} \sum_{i=1}^{n} (M_{2i-1}\delta_{2i-1}' + M_{2i}\delta_{2i}') = 0$, or the form

$$\varphi_0(x) = R_0\delta_0 + R_A\delta_A + f_0(x)$$

$$- \lim_{n\to\infty} \sum_{i=1}^{n} a_{2i-1}\left(\delta'_{2i-1} - \delta'_{2i}\right). \tag{20}$$

The distributions (19) and (20) are equivalent. It is easy to notice (Fig. 5), that

$$\lim_{n\to\infty} \sum_{i=1}^{n} \Delta S_i^{**} = \lim_{n\to\infty} \sum_{j=1}^{n} \Delta S_j^{*} = \frac{1}{2}\int_a^b h(x)\,\mathrm{d}x. \tag{21}$$

We integrate the distribution (20) twice and obtain

$$\varphi_1(x) = R_0H_0 + f_1(x) + R_AH_A - \lim_{n\to\infty} \sum_{i=1}^{n} a_{2i-1}(\delta_{2i-1} - \delta_{2i}), \tag{22}$$

$$\varphi_2(x) = (x-0)R_0H_0 + f_2(x) + (x-l)R_AH_A - \lim_{n\to\infty} \sum_{i=1}^{n} a_{2i-1}(H_{2i-1} - H_{2i});$$

$$M_{2i-1} = a_{2i-1}. \tag{23}$$

Let us assume that

$$a_{2i-1} := 2f_1(\xi_{2i-1}), \quad x_{2i-1} < \xi_{2i-1} < x_{2i},$$

$$\Delta x_{2i-1} = H_{2i-1} - H_{2i}.$$

Therefore, taking into account (21) at $h(x) = f_0(x)$ we have

$$\lim_{n\to\infty} \sum_{i=1}^{n} \Delta S_i^{*} = \lim_{n\to\infty} \sum_{i=1}^{n} \Delta S_i^{**} = \frac{1}{2}\int_a^b f_0(x)\,\mathrm{d}x \tag{24}$$

or

$$\varphi_2(x) = (x-0)R_0H_0 + f_2(x)|_{x\in\langle 0,a)} + f_2(x)|_{x\in\langle a,b\rangle} - \int_a^b f_1(x)\,\mathrm{d}x + (x-l)R_AH_A. \tag{25}$$

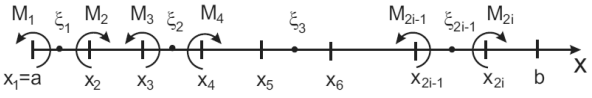

Fig. 5. Ilustration of conclusion (21).

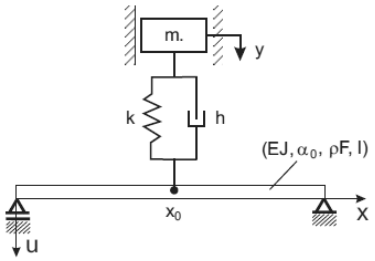

Fig. 6. Couples of forces applied in interval $\langle a, b\rangle$.

Figure 6 represents the way in which the couples of forces were applied in the interval $\langle a, b\rangle$.

From the notation of distribution (25) it issues that

$$\begin{cases} \beta y_1''(x) = (x-0)R_0H_0 + f_2(x), \\ \qquad 0 \le x < a, \\ \beta y_2''(x) = 0, \\ \qquad a \le x \le b, \\ \beta y_3''(x) = (x-0)R_0H_0 + f_2(x) + (x-l)R_AH_A, \\ \qquad b < x \le l. \end{cases} \tag{26}$$

The above reasoning indicates that the non-zero coordinate of the moment of a couple of forces at any point in the interval $a \le x \le b$ equals

$$M(x) = 2f_1(x). \tag{27}$$

It is the final proof of the equivalence of the model (17) and the model (19).

2.2. Discrete-continuous system

This part quotes the results of the study [9] which indicate the uniqueness of the models represented in Fig. 1 and Fig. 7. The following cases are considered:

1. $\alpha_0 = 0$, $h = 0$, $u(x,t) = X(x)T(t)$, $y(t) = AT(t)$;
2. $\frac{\alpha_0}{E} = \frac{h}{K}$, $u(x,t) = X(x)T(t)$, $y(t) = AT(t)$;
3. $\frac{\alpha_0}{E} \neq \frac{h}{K}$, $u(x,t) = X(x)T(t)$ — this does not lead to the goal since it is impossible to separate the variables We apply the principle of invariability eigenvalue problems for (1.), (2.) and (3.).

Figure 7 represents the model associated with the model in Fig. 1, leading to separation of variables for the case (3.).

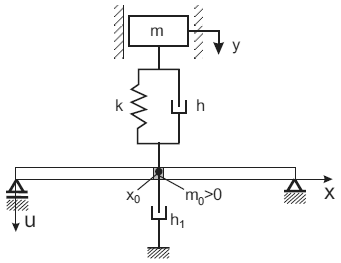

Fig. 7. Model of discrete-continous system for case (3.).

For the case (3.) we assume that

$$u(x,t) = X(x)T(t), \quad y(t) = AS(t), \quad \frac{\alpha_0}{E} \neq \frac{h}{k}, \tag{28}$$

where $X(x)$ and A are the same as in the cases (1.) and (2.)

$$h_1 = k\left(\frac{k}{h} - \frac{\alpha_0}{E}\right), \quad \frac{h}{k} - \frac{\alpha_0}{E} \neq 0$$

for the cases (1.), (2.) and (3.):

$$\begin{cases} X^{IV} - \lambda^4 X = \left(\frac{k}{\omega_0^2 - \omega^2} + \frac{m_0}{EJ}\right)\omega^2 X(x_0)\delta_{x_0}, \\ \qquad \lambda^4 = \frac{\rho F \omega^2}{EJ}, \\ \frac{X(x_0)}{A} = \frac{\omega_0^2 - \omega^2}{\omega_0^2}, \quad \omega_0^2 = \frac{k}{m} X(0) = X(l) = 0, \\ \qquad X''(0) = X''(l) = 0, \end{cases} \tag{29}$$

$$\ddot{T} + \omega^2 T = 0 \text{ for } \alpha_0 = 0,\ h = 0,$$

$$\ddot{T} + \frac{\alpha_0}{E}\omega^2 \dot{T} + \omega^2 T = 0$$

$$\text{for} \quad \frac{\alpha_0}{E} = \frac{h}{k}\ddot{T} + \frac{\alpha_0}{E}\omega^2 \dot{T} + \omega^2 T = 0$$

$$\text{for} \quad x \neq x_0 \text{ for } \frac{\alpha_0}{E} \neq \frac{h}{K}, \tag{30}$$

while for $x = x_0$ functions $S(t)$ and $T(t)$ are determined by the system of Eqs. (31):

$$\ddot{S} + 2\alpha\dot{S} + \omega_0^2 S + \left(1 - \frac{\omega^2}{\omega_0^2}\right)\left(2\alpha\dot{T} + \omega_0^2 T\right) = 0,$$

$$\ddot{T} + \left(\omega^2 + \frac{k\omega_0^2}{m_0(\omega_0^2 - \omega^2)}\right)\left(\frac{\alpha_0}{E}\dot{T} + T\right)$$

$$- \frac{k\omega_0^2}{m_0(\omega_0^2 - \omega^2)}\left(\frac{h}{k}\dot{S} + S\right) = 0. \tag{31}$$

The model shown in Fig. 7 includes also the case represented in Fig. 8, which is interesting both for theoretical

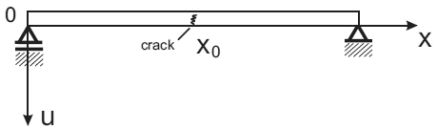

Fig. 8. Euler's beam with crack.

and practical reasons. Below there are equations of eigenfunctions $X(x)$ and time functions $T(t)$:

$$X^{IV} - \lambda^4 X = \frac{m_0}{EJ}\omega^2 \delta_{x_0},$$

$$\ddot{T} + \frac{h_1}{m_0}\dot{T} = \omega^2 T = 0 \quad \text{for } x = x_0;$$

$$\ddot{T} + \omega^2 T = 0 \quad \text{for } x \neq x_0. \tag{32}$$

2.3. Euler's beam with a transverse crack

This part discusses two models describing a crack perpendicular to the axis of Euler's beam. The crack at the point $x_0 \in (0, l)$ causes a local decrease of the cross-section area at the point x_0 and a local decrease of bending stiffness. The local decrease of the cross-section causes a local decrease of stress. The local increases of stress can also be explained with a local increase of the bending moment, which issues from the well-known formula

$$\sigma(x) = \frac{M_{\mathrm{g}}(x)}{W_{\mathrm{g}}(x)}. \tag{33}$$

2.3.1. Model one

This model describes local decrease of the cross-section and stiffness at the point x_0.

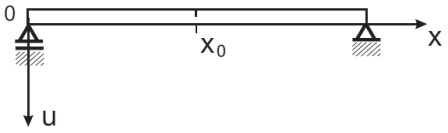

Fig. 9. A beam with a local change of cross-section at the point x_0.

The equation of the eigenfunctions of the system represented in Fig. 9 was derived from Eq. (1) and assumed the form (34):

$$X^{IV} - \lambda^4 X = \gamma_1 \Big[\sigma_1(x_0)\delta''_{x_0} + \sigma_2(x_0)\delta'_{x_0}$$

$$+ \frac{1}{1 + \gamma_1}\sigma_3(x_0)\delta_{x_0}\Big]; \quad \lambda^4 = \frac{\rho F \omega^2}{EJ}, \tag{34}$$

$-1 < \gamma_1 \leq 0$, $\sigma_i(x_0) = X^{(i)}(x_0 + \epsilon) - X^{(j)}(x_0 - \epsilon)$, $\delta^{(i)}_{x_0}$, $i = 1, 2, 3$, $\delta^{(j)}_{x_0}$, $j = 0, 1, 2$ — Dirac delta distribution and its derivatives.

2.3.2. Model two

This model, represented in Fig. 10 describes a local increase of the bending moment.

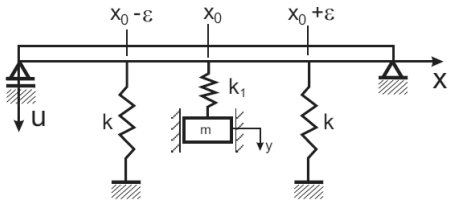

Fig. 10. A beam with a local change of the bending moments at the point x_0.

The equation of the eigenfunction of the system in the figure above has been derived in a standard way, applying the condition

$$ku(x_0 - \epsilon, t) + ku(x_0 + \epsilon, t) = k_1[y(t) - u(x_0, t)]$$

for every t.

This equation has the form (35):

$$X^{IV} - \lambda^4 X = u\frac{k}{EJ}X(x_0)\delta_{x_0}. \tag{35}$$

The initial examination of (34) and (35) indicates that it is a decrease of the initial vibration rate in both cases, which coincides with the results described in literature [7, 8]. The precise derivation of the solutions of Eqs. (34) and (35) as well as demonstration of the equivalence of the models represented in Fig. 9 and Fig. 10 will be the subject of a separate study.

3. Conclusion

The main goal of this work was investigation of these models that are simpler to describe. This models were constructed and mathematically described for three physical systems. The advantage of these models consists in the compact of the mathematical description. This form of the description can be used in the analysis of boundary problems and initial-boundary problems associated with continuous and discrete-continuous systems. For the last physical system two models were constructed, which allow us for a much easier evaluation of changes in the first vibration frequency caused by a crack. The goal of the study has been achieved.

References

[1] P. Antosik, J. Mikulski, R. Sikorski, *Theory of Distributions; the Sequential Approach*, Elsevier Sci. Publ., New York 1973.

[2] F.P. Beer, E.R. Johnson (Jr.), *Mechanics for Engineers*, Cliffs, New Jersey 1977.

[3] S. Kasprzyk, S. Sedziwy, *Bull. Acad. Sci. Math.* **31**, 329 (1983).

[4] L. Schwartz, *Mathematics for Physical Sciences, Dover Books on Mathematics*, Dover Publ., Dover 2008.

[5] S. Kasprzyk, S. Sedziwy, *Bull. Acad. Sci. Math.* **43**, 413 (1995).

[6] S. Kasprzyk, *Dynamics of Continous Systems*, Wydawnictwo AGH, Kraków 1994 (in Polish).

[7] W. Ostachowicz, M. Krawczuk, *J. Sound Vibrat.* **150**, 191 (1991).

[8] L. Majkut, *Arch. Acoust.* **31**, 17 (2006).

[9] S. Kasprzyk, *Acta Phys. Pol. A* **119**, 981 (2011).